Exergetic Evaluation of Steel Coaxial Heat Exchangers

Tobias Blanke (blanke@sij.fh-aachen.de)
FH Aachen, Bayernallee 9, 52066 Aachen, Germany https://orcid.org/0000-0003-1529-5529

Markus Hagenkamp
FH Aachen, Bayernallee 9, 52066 Aachen, Germany.

Bernd Döring
FH Aachen, Bayernallee 9, 52066 Aachen, Germany.

Joachim Göttsche
Solar Institut Jülich, FH Aachen, Heinrich-Mußmann-Str. 5, 52428 Jülich, Germany

Vitali Reger
Lehr- und Forschungsgebiet Nachhaltigkeit im Metallleichtbau, RWTH Aachen, Mies-van-der-Rohe-Straße 1, 52074 Aachen, Germany.

Markus Kuhnhenne
Lehr- und Forschungsgebiet Nachhaltigkeit im Metallleichtbau, RWTH Aachen, Mies-van-der-Rohe-Straße 1, 52074 Aachen, Germany.

Research

Keywords: geothermal heat exchanger, heat exchanger, annular, coaxial, hydraulic, thermal, exergy, optimization, steel

Posted Date: January 29th, 2021

DOI: https://doi.org/10.21203/rs.3.rs-153774/v1

Version of Record: A version of this preprint was published at Geothermal Energy on July 26th, 2021. See the published version at https://doi.org/10.1186/s40517-021-00201-3.

RESEARCH

Exergetic evaluation of steel coaxial heat exchangers

Tobias Blanke[1*†], Markus Hagenkamp[1†], Prof. Dr. Bernd Döring[1], Dr. rer. nat. Joachim Göttsche [2], Vitali Reger[3] and Prof. Dr. Markus Kuhnhenne[3]

*Correspondence:
blanke@sij.fh-aachen.de
[1]FH Aachen, Bayernallee 9, 52066 Aachen, Germany
Full list of author information is available at the end of the article
†Equal contributor

Abstract

Background: A proven option to found buildings are geothermally activated steel pipes. Statics determine their dimensions. Energy improvement research focuses on the radius of inner pipe of such coaxial geothermal probes. Mass flow rate is often constant when optimizing inner pipe dimensions. In contrast, in this study flow conditions in outer pipe are constant (constant Reynolds number) to ensure that they not change during optimization. Aim is to maximize net exergy difference for the desired flow type by changing inner pipe radius (after deduction of hydraulic effort). System technology can be selected based on this optimal design and its associated boundary conditions for mass flow and temperatures.

Methods: Thermal calculations based on Hellström are carried out to quantify an influence of changing inner pipe radius on thermal yield. A hydraulic optimization of inner pipe radius is performed. Increasing inner pipe radius results in decreasing hydraulic losses in inner pipe but increases hydraulic losses in outer circular ring. Net exergy difference is a key performance indicator to combine thermal and hydraulic effects. Optimization of net exergy difference is carried out for selected scenarios. All calculations are based on various, but fixed Reynolds numbers in the circular ring ($Re = [4e3, 1e4, 1e5]$), instead of fixed mass flow rates. This ensures fixed flow conditions and no unnecessary high mass flow rate.

Results: Optimal inner radius is approximately as large as outer radius considering thermal results. Reynolds numbers are always bigger in inner pipe, due to the constant Reynolds number in circular ring. Both indicate that from a thermal point of view, a high mass flow rate and a high degree of turbulence are particularly important. Hydraulic optimal inner pipe radius is $54\,\%$ of outer pipe radius for laminar flow scenarios and $60\,\%$ for turbulent flow scenarios. Exergetic optimization shows a predominant influence of hydraulic losses, especially for small temperature gains.

Conclusions: Design of coaxial geothermal probes should focus on the hydraulic optimum and take energetic optimum as a secondary criterion to maximize net exergy difference.

Keywords: geothermal heat exchanger; heat exchanger; annular; coaxial; hydraulic; thermal; exergy; optimization; steel

1 Introduction

Steel pipes are well suited to found buildings on unreliable ground [1]. The boreholes must be drilled in in such cases to ensure the static requirements of the building. It is reasonable to use them for geothermal purposes, too. Steel pipes can be geothermally activated for example by using them as a single or double U geothermal probe [2].

Another option are coaxial pipes [3, 4]. Main advantages of coaxial pipes are a fully thermally activated steel pipe and avoidance of concrete use. Since the steel pipe is designed by static purposes their outer dimensions are fixed. So, improvement options are limited to the inner pipe. In particular, the inner radius can serve as a primary parameter for thermal, hydraulic and exergetic optimization purposes.

Previous studies have researched the influence of inner pipe radius considering thermal [5, 6] or hydraulic perspectives [5, 7]. Combined thermal and hydraulic research based on exergy has not yet been done. Thermal studies have shown, that inner pipe radius and mass flow rate should be as big as possible [5, 6]. A hydraulic optimal inner pipe radius has been proposed to be about 0.65 times the outer pipe radius for turbulent flows [5, 7] and 0.68 for laminar flows [7]. Here a constant mass flow rate is assumed, and different pipe surface roughness's are neglected.

In this study, optimization is based on constant Reynolds numbers to ensure comparable flow conditions. So, flow conditions are either sure laminar or turbulent in the circular ring, which cannot be guaranteed with a constant mass flow. The mass flow rate is set as minimal as possible to ensure required flow conditions. So, no unnecessary hydraulic loss is caused. In this study the Reynolds number in the circular ring is kept constant to ensure that the flow is either laminar or turbulent. The mass flow depends on inner pipe radius and Reynolds number and is not constant during calculations.

Thermal and hydraulic calculations are carried out. The difference to existing literature is pointed out, especially for the hydraulic perspective. Influence of surface roughness on the hydraulic optimum is investigated. To obtain a general result, the thermal and hydraulic influences are compared based on an optimization of the exergetic sum. Aim is to derive a more general statement than in previous publications on the optimal dimensioning of coaxial heat exchangers based on comparable flow conditions and exergy.

2 Methodology

Figure 1 shows a sketch of a foundation pile with a coaxial heat exchanger and the corresponding geometric parameters. These are: the inner radius of the inner pipe ($\overline{r_i}$), an inner pipe thickness (δ), outer radius of inner pipe (r_i), inner radius of outer pipe (r_a) and outer pipe radius of outer pipe (r_o) as well as thermal conductivity of inner pipe (λ_p) and outer pipe (λ_c).

In table 3 the parameter values for all calculations are shown. To ensure the generalizability of the results dimensionless variables are defined. These are: a dimensionless inner radius (c), a dimensionless mean inner radius (c_m) and Standard Dimension Ratio (SDR) based on [8]. They are defined as follows:

$$c = \frac{r_i}{r_a} \tag{1}$$

$$c_m = \frac{r_i - \frac{\delta}{2}}{r_a} \tag{2}$$

$$SDR = \frac{2 \cdot r_i}{\delta} \tag{3}$$

The Reynolds number for circle ring (Re_c) and inner pipe (Re_p) are defined by the following equations [9]:

$$Re_c = \frac{v_c \cdot d_{hyd,c}}{\nu} = \frac{\dot{m} \cdot 2 \cdot r_a \cdot (1-c)}{\rho \cdot \nu \cdot \pi \cdot (1^2 - c^2) \cdot r_a} = \frac{2 \cdot \dot{m}}{\rho \cdot \nu \cdot \pi \cdot r_a \cdot (1+c)} \tag{4}$$

using

$$d_{hyd,c} = 2 \cdot (r_a - r_i) \tag{5}$$

$$Re_p = \frac{v_p \cdot d_{hyd,p}}{\nu} = \frac{\dot{m} \cdot 2 \cdot r_a \cdot \frac{\overline{r_i}}{r_a}}{\rho \cdot \nu \cdot \pi \cdot r_a^2 \cdot \left(\frac{\overline{r_i}}{r_a}\right)^2} = \frac{2 \cdot \dot{m}}{\rho \cdot \nu \cdot \pi \cdot r_a \cdot c \cdot \left(1 - \frac{2}{SDR}\right)} \tag{6}$$

using

$$d_{hyd,p} = 2 \cdot \overline{r_i} \tag{7}$$

2.1 Thermal calculations

The concept of borehole resistances by Hellström is used for thermal calculations [10]. First considered resistance is internal borehole resistance (R_a) to model thermal short circuit heat transfer. Second resistance is borehole resistance (R_b) as an indicator for collected heat from the ground. For coaxial geothermal pipes the internal borehole resistance R_a is defined by [10] as:

$$R_a = \frac{1}{2 \cdot \pi \cdot c \cdot \left(1 - \frac{2}{SDR}\right) \cdot r_a \cdot \alpha_i(c)} + \frac{\ln\left(\frac{1}{1-\frac{2}{SDR}}\right)}{2 \cdot \pi \cdot \lambda_p} + \frac{1}{2 \cdot \pi \cdot c \cdot r_a \cdot \alpha_o(c)} \tag{8}$$

Borehole resistance R_b is defined by [10]:

$$R_b = \frac{1}{2 \cdot \pi \cdot r_a \cdot \alpha_o(c)} + \frac{\ln\left(\frac{r_o}{r_a}\right)}{2 \cdot \pi \cdot \lambda_c} \tag{9}$$

Total borehole resistance (R_b^*) combines both influences and is defined by [11, 12] as follows:

$$R_b^*(c) = R_b(c) + \frac{L^2}{3 \cdot R_a(c) \cdot \dot{m}(c)^2 \cdot c_p^2} \tag{10}$$

Total borehole resistance (R_b^*) combines both influences and is defined by [11, 12] as follows: with L as borehole depth, mass flow rate $\dot{m}$ and heat capacity c_p. α_i and

α_o are the convective heat transfer coefficients of the inner pipe and outer circular ring, respectively.

Best thermal performance corresponds to lowest total borehole resistance (R_b^*) since there are no other ways of heat transmission (radiation, further convective processes...) to be considered. Convective heat transfer coefficients are calculated by using Nusselt number Nu [13]:

$$Nu_k = \frac{\alpha_k \cdot d_{hyd,k}}{\lambda_{fl}} \tag{11}$$

with the hydraulic diameter $d_{hyd,k}$ for $k \in \{c, p\}$ and the thermal conductivity of the fluid λ_{fl}.

The Nusselt number calculation differs between laminar flow and turbulent flow as well as between round pipes and circular rings. Nusselt number is calculated according to Gnielinski [13]. Nusselt depends on Prandl number, Reynolds number, inner to outer pipe radius, different radii and borehole length.

For thermal calculations a reference case (Index st.) is defined based on [4]. In order to analyze sensitivities, every parameter in the reference case is varied. Parameter values and variation ranges can be found in Table 1.

2.2 Hydraulic optimization

Objective for the hydraulic optimization is to minimize power demand caused by hydraulic losses due to fluid friction. These hydraulic losses are directly dependent on the mass flow in the coaxial heat exchanger.

Power demand (P) for a volume flow rate ($\dot{V}$) or mass flow rate ($\dot{m}$) in a coaxial heat exchanger with hydraulic losses (Δp_{coax}) is defined as [14]:

$$P = \Delta p_{coax} \cdot \dot{V} = \Delta p_{coax} \cdot \frac{\dot{m}}{\rho} \tag{12}$$

Hydraulic losses in the heat exchanger can be calculated based on equation 13 [14]:

$$\Delta p_{coax} = \left[\frac{\Psi_c}{d_{hyd,c}} \cdot v_c^2 + \frac{\Psi_p}{d_{hyd,p}} \cdot v_p^2 \right] \cdot \frac{\rho}{2} \cdot L \tag{13}$$

with

Ψ_p	friction factor of inner pipe
Ψ_c	friction factor of circular ring
$d_{hyd,p}$	hydraulic diameter of inner pipe
$d_{hyd,c}$	hydraulic diameter of circular ring
v_p	fluid velocity in inner pipe
v_c	fluid velocity in circular ring
ρ	density of fluid
L	length of geothermal pipe

The resulting equation is with the hydraulic diameter (s. Equations 5,7) and the dependency between mass flow rate, cross sectional area ($A = \pi \cdot r^2$) and velocity

v ($v = \frac{\dot{m}}{\rho \cdot A}$):

$$\Delta p_{coax} = \left[\frac{\Psi_c}{2 \cdot (r_a - r_i)} \cdot \left(\frac{\dot{m}}{\rho \cdot \pi \cdot (r_a^2 - r_i^2)} \right)^2 + \frac{\Psi_p}{2 \cdot (r_i - \delta)} \cdot \left(\frac{\dot{m}}{\rho \cdot \pi \cdot (r_i - \delta)^2} \right)^2 \right] \cdot \frac{\rho}{2} \cdot L \tag{14}$$

Reynolds numbers of the circular ring are fixed at $Re_{c,lam} = 1000$ for laminar flows based on [15] and $Re_{c,turb} = 10\,000$ for turbulent flows based on [13] to ensure a good thermal response. The mass flow rate as a function of Reynolds number can be calculated with:

$$\begin{aligned} Re_c &= \frac{v_c \cdot d_{hyd,c}}{\nu} = \frac{\frac{\dot{m}}{\rho \cdot \pi \cdot (r_a^2 - r_i^2)} \cdot 2 \cdot (r_a - r_i)}{\nu} = \frac{2 \cdot \dot{m}}{\rho \cdot \pi \cdot \nu \cdot (r_a + r_i)} \\ \Leftrightarrow \dot{m} &= \frac{Re_c \cdot \rho \cdot \pi \cdot \nu \cdot (r_a + r_i)}{2} \end{aligned} \tag{15}$$

Hydraulic losses can be calculated using the resulting mass flow rate (equation 15) in equation 14:

$$\begin{aligned} \Delta p_{coax} &= \left[\frac{\Psi_c}{2 \cdot (r_a - r_i)} \cdot \frac{\rho}{2} \cdot \left(\frac{Re_c \cdot \rho \cdot \pi \cdot \nu \cdot (r_a + r_i)}{2 \cdot \rho \cdot \pi \cdot (r_a^2 - r_i^2)} \right)^2 \right. \\ &\quad \left. + \frac{\Psi_p}{2 \cdot (r_i - \delta)} \cdot \frac{\rho}{2} \cdot \left(\frac{Re_c \cdot \rho \cdot \pi \cdot \nu \cdot (r_a + r_i)}{2 \cdot \rho \cdot \pi \cdot (r_i - \delta)^2} \right)^2 \right] \cdot L \\ &= \left[\frac{\rho \cdot (Re_c \cdot \nu)^2}{16} \left(\frac{\Psi_p \cdot (r_a + r_i)^2}{(r_i - \delta)^5} + \frac{\Psi_c}{(r_a - r_i)^3} \right) \right] \cdot L \end{aligned} \tag{16}$$

The resulting power demand is:

$$\begin{aligned} P &= \Delta p_{coax} \cdot \dot{V} \\ &= \left[\frac{\rho \cdot L \cdot (Re_c \cdot \nu)^2}{16} \left(\frac{\Psi_p \cdot (r_a + r_i)^2}{(r_i - \delta)^5} + \frac{\Psi_c}{(r_a - r_i)^3} \right) \right] \cdot \frac{\frac{Re_c}{2} \cdot \rho \cdot \pi \cdot \nu \cdot (r_a + r_i)}{\rho} \end{aligned} \tag{17}$$

The equation can be simplified using dimensionless inner pipe radius (c) and Standard Dimension Ratio (SDR):

$$P = \frac{\rho \cdot \pi \cdot L \cdot (Re_c \cdot \nu)^3}{32 \cdot r_a^2} \cdot \left(\frac{\Psi_p \cdot (1 + c)^3}{c^5 \cdot \left(1 - \frac{2}{SDR}\right)^5} + \frac{\Psi_c \cdot (1 + c)}{(1 - c)^3} \right) \tag{18}$$

Density (ρ), critical Reynolds number (Re_c), kinematic viscosity (ν) and outer pipe radius (r_a) are assumed to be constant:

$$P = C \cdot \left(\frac{\Psi_p \cdot (1 + c)^3}{c^5 \cdot \left(1 - \frac{2}{SDR}\right)^5} + \frac{\Psi_c \cdot (1 + c)}{(1 - c)^3} \right) \tag{19}$$

With these assumptions a dimensionless power factor (K) can be defined:

$$K \coloneqq \frac{P}{C} = \frac{\Psi_p \cdot (1+c)^3}{c^5 \cdot \left(1 - \frac{2}{SDR}\right)^5} + \frac{\Psi_c \cdot (1+c)}{(1-c)^3} \tag{20}$$

Minimization of the dimensionless power factor (K) is sufficient to minimize power demand. Consequently the final objective function is defined by equation 21 for the hydraulic minimization problem.

$$\min\left[K(c)\right]_{\forall c \in (0,1)} = \min\left[\frac{\Psi_p \cdot (1+c)^3}{c^5 \cdot \left(1 - \frac{2}{SDR}\right)^5} + \frac{\Psi_c \cdot (1+c)}{(1-c)^3}\right]_{\forall c \in (0,1)} \tag{21}$$

The derivative of the objective function results in a polynomial function of grade 6. An analytical solution to the minimization problem is impractical. A numerical approach is chosen based on a Sequential Quadratic Programming (SQP) algorithm implemented in Matlabs 'fmincon' function [16]. More information on SQP as "one of the most effective methods for nonlinearly constrained optimization problems" can be found in [17],[18]. A Matlab script is set up to evaluate the optimization problem for several parameter sets (see Table 5 for all scenarios).

Initial value of c for minimization in all scenarios is set to $c_0 = 0.9$. This is nearly the end of valid range and resulting in good gradients for minimization.

The friction factors are unknown. Three cases are evaluated to estimate feasible values. These cases are: laminar flow (laminar), turbulent flow outside rough regime (turb.) and rough regime turbulent flow (turb. r.r.).

For the laminar flow case the friction factors for pipe (Ψ_p) and circular ring (Ψ_c) are defined according to [19] as:

$$\Psi_p = \frac{64}{Re_p} \tag{22}$$

$$\Psi_c = \frac{64}{Re_c} \cdot \frac{(1-c)^2 \cdot \left(1-c^2\right)}{1 - c^4 - \frac{(1-c^2)^2}{\ln(1/c)}} \tag{23}$$

Ratio of the Reynolds numbers for pipe (Re_p) and circle ring (Re_c) can be formulated as:

$$\frac{Re_c}{Re_p} = \frac{c \cdot \left(1 - \frac{2}{SDR}\right)}{1+c} \tag{24}$$

The resulting minimization function by inserting equations 22 and 23 in 21 is:

$$\begin{aligned} &\min\left[K(c)\right]_{\forall c \in (0,1)} \\ &= \min\left[\frac{(1+c)^2}{c^4\left(1 - \frac{2}{SDR}\right)^4} + \frac{(1+c)}{(1-c)^3} \cdot \frac{(1-c)^2 \cdot \left(1-c^2\right)}{1 - c^4 - \frac{(1-c^2)^2}{\ln\left(\frac{1}{c}\right)}}\right]_{\forall c \in (0,1)} \end{aligned} \tag{25}$$

For turbulent flows in the circular ring and inner pipe the friction factor can be calculated with [20]:

$$\frac{1}{\sqrt{\Psi}} = -2 \cdot \log\left(\frac{2.51}{Re \cdot \sqrt{\Psi}} + \frac{k}{3.72 \cdot d_{hyd}}\right) \quad \text{(outside rough regime)} \tag{26}$$

$$\frac{1}{\sqrt{\Psi}} = -2 \cdot \log\left(\frac{k}{3.72 \cdot d_{hyd}}\right) \quad \text{(in rough regime)} \tag{27}$$

The hydraulic diameters can be written as a function of the inner radius of the outer pipe (r_a):

$$d_{hyd,p} = \left(1 - \frac{2}{SDR}\right) \cdot c \cdot 2 \cdot r_a \tag{28}$$

$$d_{hyd,c} = (1 - c) \cdot 2 \cdot r_a \tag{29}$$

Surface roughness of inner pipe (k_p) and outer pipe (k_a) are used to define a medium surface roughness (k_c) for the circular ring. This is based on circumference:

$$k_c := \frac{k_a \cdot 2\pi \cdot r_a + k_p \cdot 2\pi \cdot r_i}{2\pi \cdot (r_a + r_i)} = \frac{k_a + c \cdot k_p}{1 + c} \tag{30}$$

An iterative solution of equation 26 for Ψ is necessary to formulate friction factors outside the rough regime. It is carried out programmatically. In both cases, the resulting friction factors can be used in equation 21 to complete the objective function for optimization.

Similar to the thermal calculations a range of variations is carried out for sensitivity and validation purposes (s. table 2). Values for SDR are chosen according to EN 12201-2 [8].

2.3 Exergy difference maximization

In practical applications thermal effects cannot be evaluated properly if hydraulic effects are neglected and vice versa. For a combined analysis, exergy is an appropriate indicator.

An exergy optimization is carried out using exergy balance by Lee [21]:

$$\max(\dot{E}_{ex})_{\forall c \in (0,1)} = \max\left(\left(1 - \frac{T_e \cdot \ln\left(\frac{T_{in}}{T_{out}}\right)}{T_{in} - T_{out}}\right) \cdot \dot{Q}_{geo} - P_{hydr}\right)_{\forall c \in (0,1)} \tag{31}$$

Hydraulic power (P_{hydr}) is calculated as explained in section 2.2. Heat flux ($\dot{Q}_{geo}$) and outlet Temperature (T_{out}) are calculated as explained in equation 32 and 34, respectively. Earth Temperature (T_e) is assumed to be 10 °C and inlet Temperature (T_{in}) depends on the considered case explained later.

The heat flux of coaxial heat exchanger is defined as difference in enthalpy flow of inlet and outlet [13]:

$$\dot{Q}_{geo} = \dot{m} \cdot c_p \cdot (T_{in} - T_{out}) \tag{32}$$

The heat flux entering the system must equal the heat flux leaving the system, considering a stationary system. $\dot{Q}_{geo}$ can therefore be calculated based on [10] with a linearized fluid temperature. Resulting error is less then 10^{-6} compared to a logarithmic temperature:

$$\dot{Q}_{geo} = \frac{L \cdot \left(\frac{T_{in}+T_{out}}{2} - T_e\right)}{R_b^* + R_g} \tag{33}$$

with R_g as thermal ground resistance and R_b^* as total borehole resistance calculated as explained in section 2.1. Combining equations 32 and 33 yields to:

$$T_{out} = \frac{\left(\dot{m} \cdot c_p - \frac{L}{2 \cdot \left(R_b^* + R_g\right)}\right) \cdot T_{in} + \frac{L}{R_b^* + R_g} \cdot T_e}{\dot{m} \cdot c_p + \frac{L}{2 \cdot R}} \tag{34}$$

The optimization uses the same optimizing algorithm as in section 2.2. Starting point is c=0.8. Calculation is done for SDR values from 6 to 41 and thermal ground resistance (R_g) values from 0.05 m K/W to 0.3 m K/W. An inlet temperature difference above earth temperature of $\Delta T = T_{in} - T_e = 5\,\mathrm{K}$ and ΔT =20 K is assumed for laminar flows. ΔT =20 K as well as ΔT =50 K above earth temperature is assumed for turbulent flows.

3 Results and discussion

3.1 Thermal results

Figure 2 illustrates that in the laminar case the total borehole resistance decreases with an increasing dimensionless inner radius (c). This trend is independent of the considered case. Equation 4 shows that an increasing dimensionless inner radius results in an increasing mass flow rate, if Re_c is kept constant. Additionally equation 24 shows the ratio between inner pipe and circular ring Reynolds number, which is constantly decreasing with an increasing dimensionless inner radius (c). This results in lower Reynolds numbers in the inner pipe for larger dimensionless radii c. Since lower Reynolds numbers inhibit heat transfer, the thermal short circuit heat flux is expected to decrease with increasing dimensionless inner radii (c). Therefore, it is plausible that the thermal performance increases constantly towards $c \approx 1$. Total borehole resistance for turbulent flow scenarios is increasing with dimensionless inner radius to its maximum at about $c = 0.3$. It decreases from there until the minimum is reached close to a dimensionless inner radius of $c = 1$. The initial increase in the resistance appears to be due to calculation inaccuracies for small dimensionless inner pipe radii in the turbulent case. So even for turbulent cases the conclusion holds that for best thermal performance, the greatest possible dimensionless inner radius should be chosen.

For both SDR variations, R_b^* differs on average by less than 0.3 % and at most by 3 % from the standard case. Influence of SDR on the thermal response is therefore neglected in further calculations and not shown in the graphs (see Table 4).

3.1.1 Material

Laminar results for the standard case (inner pipe: plastic, outer pipe: steel) differ only slightly from results where the inner pipe material is changed to steel as well (average difference of 1.8 %). In the switched case (outer pipe made from plastic and an inner pipe made of steel), results coincide in good approximation to the results of plastic as material for both pipes. Generally, when a plastic pipe is used as outer pipe, total borehole resistance is more than 90 % higher than in the standard case due to lower thermal conductivity. These findings suggest that the influence of outer pipe material on the thermal response is by far greater than the influence of inner pipe material. To ensure good readability of the results only the standard case and the case with switched materials are plotted in figure 2 a). In turbulent flows an outside pipe of plastic results in an on average 25 times higher borehole resistance.

3.1.2 Borehole radius

An increased borehole radius in laminar flows results in an on average 27 % lower total borehole resistance. A decrease in borehole radius results in a 16 % higher total borehole resistance on average (see Fig.2 b)). In turbulent flow cases borehole radius has with +3.5 %/-14 % a less important influence on total borehole resistance than in laminar flows. Increasing outer borehole radius is beneficial for all flow types. This was to be expected since larger radius also means greater area for heat transfer per meter borehole.

3.1.3 Borehole length

For a borehole length of 100 m total borehole resistance is on average 52 % higher and for a length of 5 m on average 29 % lower for laminar case (see Fig.2 c)). This is a reasonable result since total borehole resistance is relative to unit length of the borehole. So while the thermal yield increases with borehole length it does not increase linearly, since heat loss from up- to downstream per unit length of the borehole increases (see equation 10). This is due to larger temperature differences between inner and outer pipe for greater borehole length. For turbulent flows the trend is the same. However, with an average difference of +4.1 %/-3.0 % borehole length has a significant smaller influence than in laminar flows.

3.1.4 Flow type

Increasing the Reynolds number and therefore pushing the fluid flow towards turbulent flow significantly improves the thermal response. Turbulent cases have lower total borehole resistances which is on average 13 % of the total borehole resistance in laminar cases (see Fig.2 d)). Even when the flow is already turbulent an increase in Reynolds number still yields improvements (on average $\approx$ 71 % better results for an increase in Reynolds number of one order of magnitude) that outweigh improvements by an increased borehole radius ($\approx$ 16 % better results for an radius increase of 320 %) or shorter pipes ($\approx$ 4 % better results for 1/4 of original pipe length) by far. Hence, one of the major influences on thermal performance is the flow type in the probe. The variation in the curve is reduced, when Reynolds is increased suggesting that performance is becoming independent from inner dimensionless radius and more depending on materials.

3.2 Hydraulic results

Hydraulic results are shown on figure 4. In contrast to thermal considerations the hydraulic optimization results in an optimal ratio (c). This can be explained by increasing hydraulic losses in the circular ring for large values of c and increasing hydraulic losses in the inner pipe for small values of c.

3.2.1 SDR

Results in Fig. 3 a) show an reciprocally proportional decreasing optimal inner to outer pipe ratio (c_{opt}) with an increasing Standard Dimension Ratio (SDR). This is partly due to the fact, that dimensionless inner pipe radius c_{opt} is defined as outer radius of inner pipe. So, when inner pipe thickness decreases (SDR increase), the outer radius of inner pipe decreases as well. Subtracting half of dimensionless pipe thickness from c_{opt} yields $c_{m,opt}$ as a measurement for inner pipes middle radius. Figure 3 a) shows, that the dimensionless middle radius of the inner pipe in fact increases with SDR for turbulent flows. In all cases it converges towards the outer radius of inner pipe for very big SDR values or small pipe thicknesses. For SDR values close to 2 (inner pipe thickness close to r_i), $c_{m,opt}$ converges towards 0.5 in all scenarios, meaning that the middle radius of inner pipe is $r_a/2$ and the inner pipe completely fills the room in the outer pipe($r_i = r_a$). In practice, only the outer radius of inner pipe is used for comparison. Therefore, only c_{opt} is considered in the following examinations.

3.2.2 Flow type

Laminar flows result in an optimal inner to outer pipe ratio (c_{opt}) of ca. 0.55 for big Standard Dimension Ratios (SDR), for turbulent flows the ratio is ca. 0.60 and for rough regime turbulent flows it is ca. 0.64. As discussed in Section 3.1, the Reynolds number in the inner pipe decreases with increasing c. The fact that c_{opt} is bigger for more turbulent flow types suggests, that it is advantageous not to transfer the increase in the Reynolds number of the circular ring to the inner pipes Reynolds number.

3.2.3 Material Roughness

Figure 3 b) plots the optimal dimensionless inner radius c over SDR. It is done for the flow types rough regime turbulent flow and turbulent flow as well as for all possible material combinations. The same pipe material on outer and inner pipe results for plastics in a lower optimal c than steel for turbulent flow types. When a combination of the two materials is used, then the optimum radius is not between the optima of individual materials. Instead, the optimum in the standard case (i.e. with plastic as inner pipe material) shifts significantly towards smaller radii compared to the optima of solely steel or plastic set-ups. In the switched case (with steel as inner pipe material) the optimum shifts towards larger radii. This can be explained by the following connection:

Equation 30 defines the roughness in the circular ring as a mean roughness in between both materials roughness's. When the material with smaller roughness is used for inner pipe (plastic or standard case) the roughness in inner pipe is certainly

smaller than in the circular ring. On the other hand, roughness in circular ring is smaller than in the inner pipe when steel is used for the inner pipe (switched case). For different materials the optimal dimensionless inner radius shifts in order to increase the hydraulic diameter for the section with higher material roughness. By doing so, the influence of wall roughness on the overall flow is reduced. This is because wall roughness only has an effect on flow regions close to the wall. In addition, the shift increases the velocity in the section with low wall friction and reduces it in the area with higher friction. The influence of different pipe materials is greater in rough regime turbulent flows, since friction losses are higher than in not rough turbulent flows.

3.2.4 Outer pipe radius

Results in table 5 and figure 3 c) show that the outer radius of outer pipe does not have a significant influence on the optimal dimensionless inner pipe radius. When the same material is used for inner and outer pipe, the change in c resulting from different outer pipe radii does not exceed 0.004. Where the materials of inner and outer pipe differ, there is a small shift of c (maximum: $\Delta c = 0,03$). For steel as outer pipe material (standard case) this effect is directed towards bigger radii for bigger outer pipe radii. For plastics as outer pipe material (switched case) the shift is smaller and directed towards smaller radii.

In the switched case, the quotient of the friction factors Ψ_p/Ψ_c decreases very slightly towards 1 (equal friction factors in inner pipe and circular ring) with increasing r_a. Consequently, the influence of roughness on optimal radius decreases as well. For the standard case, Ψ_p/Ψ_c increases very slightly from below 1 towards equal friction factors with increasing r_a. Here this indicates a decreasing influence of different material roughness with increased outer pipe radius. The shift is increasing very slightly with SDR, since this also means an increase in effective radius. The effect is more significant in turbulent flows than in rough regime turbulent flows because the initial influence of different material roughness is larger.

3.2.5 Approximations

Equation 35 shows an approximation to calculate the optimal dimensionless inner pipe radius for laminar flows. Approximation has a root mean square error (RMSE) less than 0.0011. The y axis intercept of 0.5367 is lower compared to Yekoladio with an intercept of 0.683 [7]. This is because Yekoladio is considering a constant mass flow rate for optimization instead of a constant Reynolds number. A clear dependency on standard dimension ratio (inner pipe thickness) is evident.

$$c_{opt,lam} = \frac{0.5604}{SDR} + 0.5367 \tag{35}$$

Equation 36 shows an approximation to calculate the optimal inner to outer pipe radius for turbulent flows. The approximation has an root mean square error less than 0.0226 for plastic pipes (switched case) and less than 0.0430 for steel pipes

(standard case). RMSE is less than 0.0070 for GHEs with both pipes made from steel and an RMSE of 0.0030 for two plastic pipes.

$$c_{opt,turb} = \frac{0.6006}{SDR} + 0.6064 \tag{36}$$

Equation 37 shows an approximation to calculate the optimal inner to outer pipe radius for rough regime turbulent flows. The approximation has an RMSE less than 0.0207 if outer and inner pipe are of same material. RMSE is less than 0.0729 for GHEs with an inner pipe of plastic and outer pipe of steel (standard case) and an RMSE of 0.0303 for switched materials. In table 6 equation parameters for the different cases are shown.

$$c_{opt,turb\ r.r.} = \frac{0.6132}{SDR} + 0.5988 \tag{37}$$

For turbulent flows the intercept of 0.6064 and 0.5988 is as well lower than Nakayamas result of 0.653 [9]. An inner pipe thickness's influence on the result is also evident here.

3.3 Exergetic results

Figure 4 a) shows the deviation of optimal dimensionless inner pipe radius in exergy optimization ($c_{opt,exergy}$) from the optimum in hydraulic optimization. It is plotted over different SDR values and several thermal ground resistances (R_g) for laminar and turbulent flows. Figure 4 b) visualizes the deviation of the exergetic optimum from the hydraulic optimum. It is plotted over ground resistance R_g for different temperature levels for laminar and turbulent flows. It is evident that in all cases the optimal dimensionless inner pipe radius increases and therefore moves from the hydraulic optimum towards the thermal optimum of $c_{opt} = 1$. The greatest change in c_{opt} occurs for laminar flows with very low thermal ground resistance. Reducing ground resistance moves the optimum closer towards the thermal optimum since thermal yields are increased.

For laminar flows, c_{opt} is increased significantly more compared to the hydraulic optimum than for turbulent flows. One explanation for this is that in laminar flows the hydraulic effort is by far less than in turbulent flows. Hence the hydraulic term in laminar flows has a smaller effect on net exergy transfer compared to turbulent flows shifting the optimal dimensionless inner pipe radius more towards the thermal optimum. Figure 4 c) even shows that c_{opt} in the laminar case is shifted beyond the initially higher c_{opt} values in the turbulent case. Another indicator for the large thermal influence compared to small influence of hydraulics on the laminar optimization result is that c_{opt} is virtually independent of SDR in exergy optimization for the considered values. This implies that changing SDR has no more significant influence on the overall result for values of SDR greater than 6 (pipe thickness $\delta < r_i/3$).

For turbulent flows the dependency on SDR is also reduced, since thermal results have proven to be independent of SDR. Nonetheless the shift towards the thermal optimum is smaller in turbulent cases than in laminar cases, suggesting that hydraulic is more important for the exergetic optimum.

As can be seen in figure 4 b) the inlet temperature difference to ground temperature also has a strong influence on c_{opt}: The greater the temperature difference, the greater the shift towards the thermal optimum. This is reasonable since the temperature has no influence on the hydraulic optimum. Therefore, greater temperature differences only increase the thermal exergy resulting in a higher weighting of the thermal optimum. It is also clearly visible that the size of the shift decreases with increasing ground resistance because this inhibits thermal processes.

Figure 4 d) visualizes the optimal solution for one scenario and the distribution of solution space. It is shown that the optimal inner to outer pipe ratio (c) is following best exergetic results for different standard dimensioning ratios SDR. Furthermore, exergy flux is increasing with increasing SDR. In this case there also is a lower bound on feasible SDR values at approximately 4 since otherwise no exergy flux can be realized.

4 Conclusion

outer pipe as possible. A constant Reynolds number in the circular ring is assumed. The hydraulic optimum has been determined at an inner to outer pipe ratio of 0.54 for laminar flows and 0.6 for turbulent flows neglecting an influence of SDR. An exergetic comparison of both influences has identified a clearly predominant impact of hydraulic losses for non-ideal thermal conditions.

For practical applications the results can be generalized. Geothermal probes are operated based on seasonal changes and often used as seasonal storages as well. In most cases, environmental conditions correspond to conditions after several hours of continuous operation. Even when there has been no operation over night/day, environmental conditions do not fully regenerate to undisturbed conditions. Hence, ground resistance can be assumed to be quite high for these periods (assume $R_g > 0.15$). In practice one also aims to keep temperature difference to ground temperature low and definitely below 50 K. If we assume, that the temperature difference does not exceed 20 K in practical operations, only two cases remain:

For laminar flow the optimal dimensionless inner pipe radius is about 28 % higher when considering exergy compared to the pure hydraulic result. The optimal radius in this case depends no longer on pipe thickness, but solely on Reynolds number and ground resistance. However, laminar flow is disadvantageous regarding the thermal behavior of the probe (see section 2.1) and therefore not recommended as a design point.

In turbulent flow the optimal dimensionless inner pipe radius is deviating only about 0.4 % from the hydraulic optimum. The influence of thermal behavior on the optimal inner pipe radius is small for the design point. Conclusively the best case for designing a geothermal probe is ensuring turbulence and choosing the radius of the inner pipe solely based on the hydraulic optimum. If the optimum is in between two available pipe sizes, it is recommendable to choose the bigger pipe in order to enhance thermal performance primarily during start up periods.

The main conclusions are:

- For turbulent flow conditions hydraulic loss is more important than the thermal gain.

- The approach with a constant Reynolds number in the circular ring leads to significantly different hydraulic results compared to an approach with a constant mass flow rate.
- The optimal hydraulic inner to outer pipe radius ratio for turbulent flows is about 0.61 with an increase of $\frac{0.60}{SDR}$.

For the standard case with a steel outer pipe radius of 75 (inner radius)/85 mm (outer radius) and an inner plastic pipe with an SDR value of 11, this leads to an optimal inner pipe radius of 49.58 mm (See equation 36). If this exact diameter is not available, the next larger one should be chosen. For example a PE-100 RC pipe with a radius of 55 mm.

Declarations

Availability of data and materials

The data used to support the findings of this study are included within the article.

Competing interests

The authors declare that they have no competing interests.

Funding

This research was carried out within the project "Integral solutions for plus energy buildings 2.0 in lightweight steel construction" from the Research Association for steel Application (FOSTA), funded by the German Federal Ministry for Economic Affairs and Energy (BMWi). Open access funding provided by Projekt DEAL.

Authors' contributions

TB and MH worked on data collection, calculations and wrote the manuscript. BD and MK directed the project, providing ideas and goals as well as logistical support. VR provided useful comments and insights to improve the conceptual models. All authors proofread the manuscript and provided their comments and insights. All authors read and approved the final manuscript.

Acknowledgements

The research project IGF 28EWN / P1285 "Integral solutions for plus energy buildings 2.0 in lightweight steel construction" from the Research Association for steel Application (FOSTA), Düsseldorf, is supported by the Federal Ministry of Economic Affairs and Energy through the German Federation of Industrial Research Associations (AiF) as part of the programme for promoting industrial cooperative research (IGF) on the basis of a decision by the German Bundestag. The project is carried out at Solar Institute Jülich.

Corresponding author

Correspondence to Tobias Blanke.

Author details

[1]FH Aachen, Bayernallee 9, 52066 Aachen, Germany. [2]Solar Institut Jülich, FH Aachen, Heinrich-Mußmann-Str. 5, 52428 Jülich, Germany. [3]Lehr- und Forschungsgebiet Nachhaltigkeit im Metallleichtbau, RWTH Aachen, Mies-van-der-Rohe-Straße 1, 52074 Aachen, Germany.

References

1. Hoback AS, Truman KZ. Least weight design of steel pile foundations. Engineering Structures. 1993;15(5):379–385. Available from: https://doi.org/10.1016/0141-0296(93)90041-2.
2. Gashti EHN, Uotinen VM, Kujala K. Numerical modelling of thermal regimes in steel energy pile foundations: A case study. Energy and Buildings. 2014;69:165–174. Available from: https://doi.org/10.1016/j.enbuild.2013.10.028.
3. Reger V, Kuhnhenne M, Hachul H, Döring B, Ebbert T, Blanke T, et al. Plusenergiegebäude 2.0 in Stahlleichtbauweise. Stahlbau. 2019;88(6):522–528. Available from: https://doi.org/10.1002/stab.201900034.
4. Reger V, Kuhnhenne M, Ebbert T, Hachul H, Blanke T, Döring B. Nutzung erneuerbarer Energien durch thermische Aktivierung von Komponenten aus Stahl. Stahlbau. 2020;89(6):512–519. Available from: https://doi.org/10.1002/stab.202000031.
5. Iry S, Rafee R. Transient numerical simulation of the coaxial borehole heat exchanger with the different diameters ratio. Geothermics. 2019;77:158–165. Available from: https://doi.org/10.1016/j.geothermics.2018.09.009.
6. Zanchini E, Lazzari S, Priarone A. Improving the thermal performance of coaxial borehole heat exchangers. Energy. 2010;35(2):657–666. Available from: https://doi.org/10.1016/j.energy.2009.10.038.
7. Yekoladio PJ, Bello-Ochende T, Meyer JP. Design and optimization of a downhole coaxial heat exchanger for an enhanced geothermal system (EGS). Renewable Energy. 2013;55:128–137. Available from: https://doi.org/10.1016/j.renene.2012.11.035.

8. DIN. EN 12201-2: Plastics piping systems for water supply, and for drainage and sewerage under pressure – Part 2: Pipes; 2011.
9. Nakayama Y, Boucher RF. Introduction to fluid mechanics. Oxford and Boston: Butterworth Heinemann; 1999. Available from: http://search.ebscohost.com/login.aspx?direct=true&scope=site&db=nlebk&db=nlabk&AN=211419.
10. Hellström G. Ground heat storage: Thermal analyses of duct storage systems [Doctoral thesis]. Lund University. Lund; 1991. Available from: http://portal.research.lu.se/portal/en/publications/ground-heat-storage--thermal-analyses-of-duct-storage-systems(f60847df-a806-4b3d-9788-ca21b1d0aa2f).html.
11. Gehlin S. Thermal response test: method development and evaluation: Thermal response test: method development and evaluation [Doctoral thesis]. Luleå University of Technology. Luleå; 2002. Available from: http://www.diva-portal.org/smash/record.jsf?pid=diva2%3A991442&dswid=6936.
12. Huber A. Calculation of Borehole Heat Exchangers: Software Manual. Zürich; 2018. Available from: http://www.hetag.ch/publikationen.html.
13. VDI e V . VDI Heat Atlas. Berlin, Heidelberg: Springer Berlin Heidelberg; 2010. Available from: https://doi.org/10.1007/978-3-540-77877-6.
14. Nakayama Y, Boucher RF. Introduction to fluid mechanics. Oxford and Boston: Butterworth Heinemann; 1999. Available from: https://katalog.ub.uni-heidelberg.de/cgi-bin/titel.cgi?katkey$=$9907318.
15. Kratz AP, Macintire HJ, Gould RE. FLOW OF LIQUIDS IN PIPES OF CIRCULAR AND ANNULAR CROSS-SECTIONS; 1931. Available from: https://www.ideals.illinois.edu/bitstream/handle/2142/4352/engineeringexperv00000i00222.pdf?sequence=3.
16. MathWorks, editor. Constrained Nonlinear Optimization Algorithms; 2019. Available from: https://de.mathworks.com/help/optim/ug/constrained-nonlinear-optimization-algorithms.html.
17. Boggs PT, Tolle JW. Sequential quadratic programming for large-scale nonlinear optimization. Journal of Computational and Applied Mathematics. 2000;124(1-2):123–137. Available from: https://doi.org/10.1016/S0377-0427(00)00429-5.
18. Daras NJ. Applications of Mathematics and Informatics in Military Science. vol. 71. New York, NY: Springer New York; 2012.
19. White FM. Fluid mechanics. 7th ed. New York, NY: McGraw-Hill; 2011.
20. Moody LF, Princeton NJ. Friction Factors for Pipe Flow. Transactions of the ASME. 1944;(66):671–684.
21. Lee KC. Classification of geothermal resources by exergy. Geothermics. 2001;30(4):431–442. Available from: https://doi.org/10.1016/S0375-6505(00)00056-0.
22. pro KUHLSOLE GmbH, editor. Glykosol N: Heat transfer fluid on basis of monoethylene glycol for Technical Applications. Düren, Germany; 2016. Available from: https://prokuehlsole.de/en/products/download-data-sheets.
23. VDI. Thermal use of the underground: Fundamentals, approvals, environmental aspects; 2010-06. Available from: https://www.vdi.de/richtlinien/details/vdi-4640-blatt-1-thermische-nutzung-des-untergrunds-grundlagen-genehmigungen-umweltaspekte.

Figures

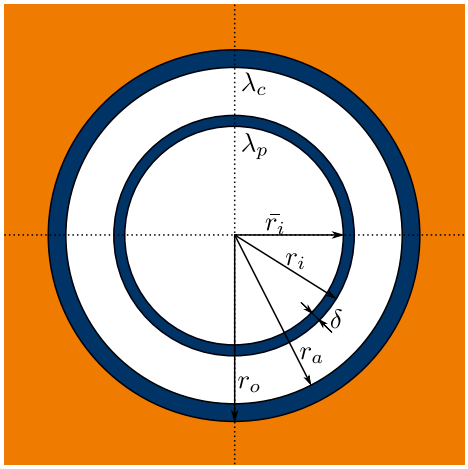

Figure 1 Sketch of a coaxial geothermal heat exchanger with an outer radius of inner pipe (r_i), an inner pipe thickness (δ), inner radius of inner pipe ($\overline{r_i}$) and an inner radius of outer pipe (r_a) as well as an inner pipe thermal conductivity (λ_p) and an outer pipe thermal conductivity (λ_c).

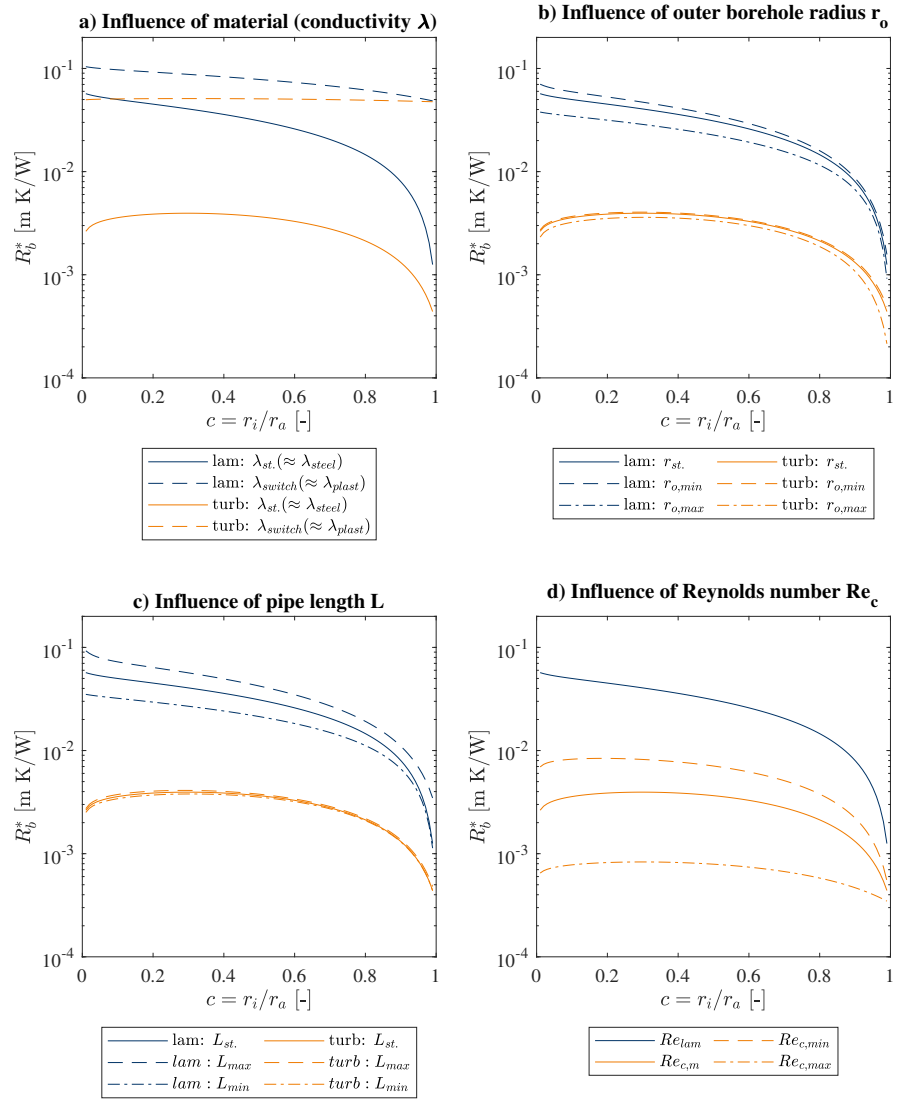

Figure 2 Thermal results Influence of several parameters on thermal performance according to [10] for laminar and turbulent flows
a) Total borehole resistance for different materials over dimensionless inner pipe radius c.
b) Total borehole resistance for different outer pipe radii r_o over dimensionless inner pipe radius c.
c) Total borehole resistance for different probe lengths L over dimensionless inner pipe radius c.
d) Total borehole resistance for different Reynolds numbers in the circular ring Re_c over dimensionless inner pipe radius c.

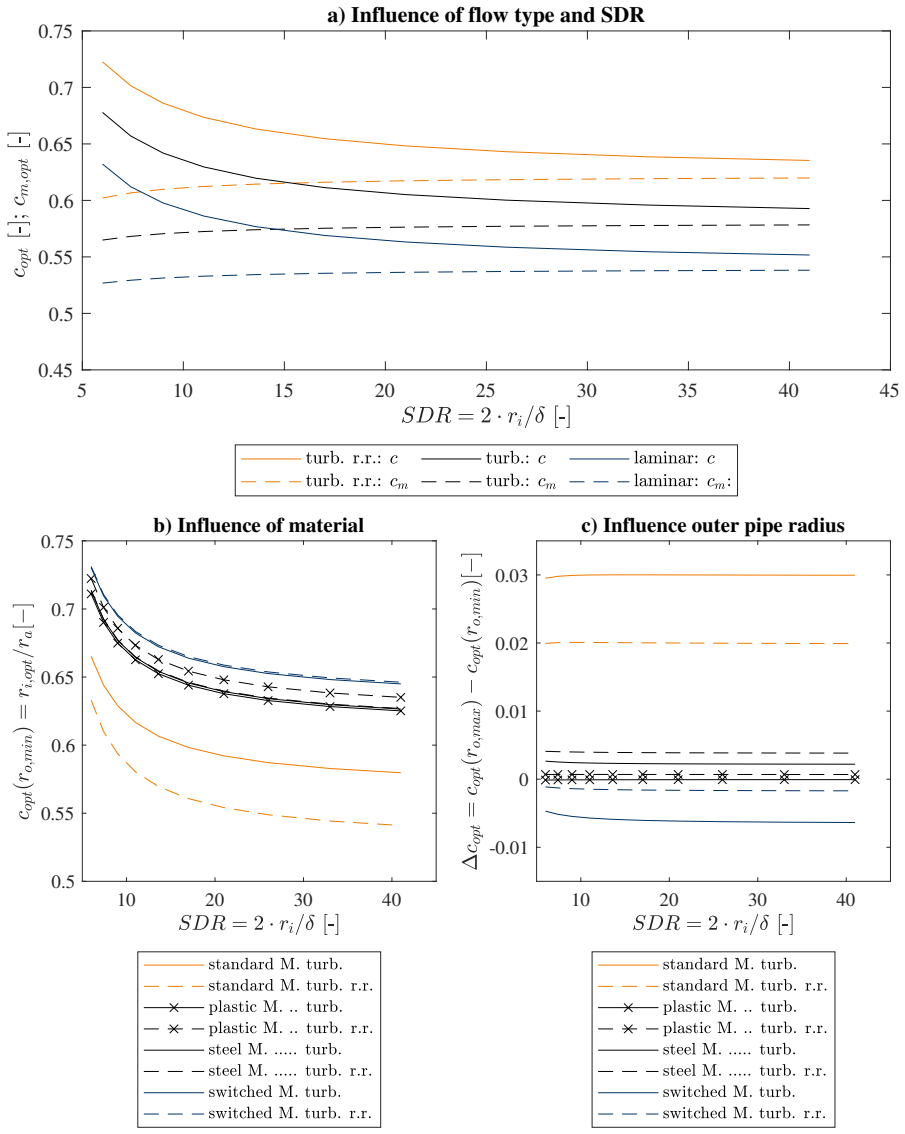

Figure 3 Results of hydraulic optimization Influence of several parameters on optimal hydraulic results for laminar and turbulent flows
a) Optimal inner pipe radius c_{opt} as well as optimal inner pipe middle radius $c_{m,opt}$ for different flow types over standard dimension ratio SDR. Reference case.
b) Optimal inner pipe radius c_{opt} calculated with the smallest outer pipe radius $r_{o,min}$ for all material combinations over SDR
c) Deviation Δc_{opt} of optimal inner pipe radius from the results in b) when calculating with the largest outer pipe radius $r_{o,max}$ for all material combinations over SDR.

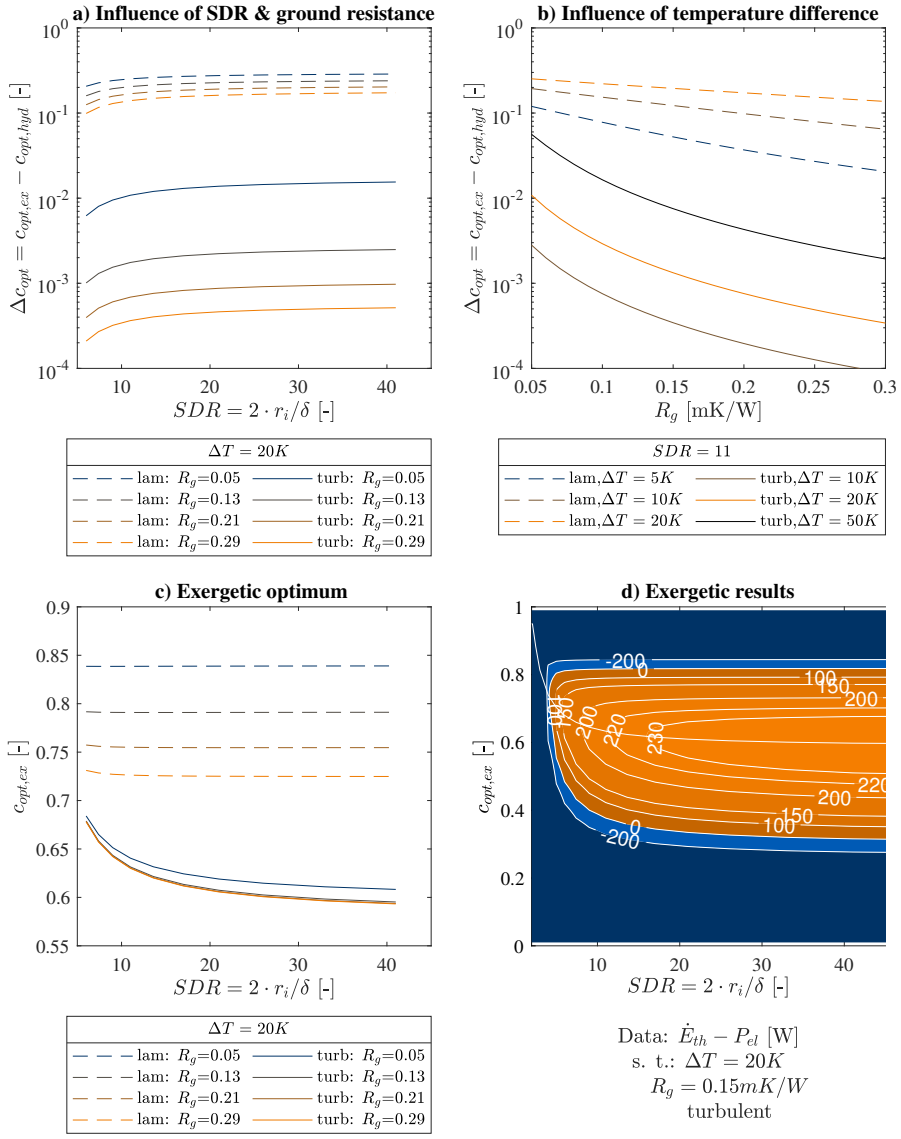

Figure 4 Exergetic results for laminar and turbulent flows
a) Change of optimal inner to outer pipe ratio (c_{opt}) compared to hydraulic results over Standard Dimension Ratio (SDR) and ground resistance (R_g)
b) Change of optimal inner to outer pipe ratio (c_{opt}) over ground resistance (R_g) and Temperature difference(ΔT).
c) optimal inner to outer pipe ratio (c_{opt}) over Standard Dimension Ratio (SDR) and ground resistance (R_g)
d) Exemplary distribution of objective function over the range of c and determined optimum c_{opt}

Tables

Table 1 Overview of modified parameters and variation range for thermal calculations

Parameter	Unit	reference case (st.)	range/Variation	Abbreviation
r_i	[m]	-	[0.01:0.99]	
SDR	[–]	11	6 41	
flow type	[–]	turbulent (turb.)	laminar turb. r. r. (rough regime)	
λ	[W/(m K)]	plastic / steel (inner/outer pipe)	steel / plastic steel / steel plastic / plastic	λ_{switch} λ_{steel} λ_{plast}
r_a	[mm]	75	39 240	$r_{a,min}$ $r_{a,max}$
r_o	[mm]	85	45 250	$r_{o,min}$ $r_{o,max}$
L	[m]	20	5 100	L_{min} L_{max}
Re	[–]	10000	1000 4000 100000	$Re_{c,lam}$ $Re_{c,min}$ $Re_{c,max}$

Table 2 Overview of modified parameters and variation range for hydraulic optimization

Parameter	Unit	reference case(st.)	range/Variation	Abbreviation
r_i	[m]	-	[0.01:0.99]	
SDR	[–]	11	6 7.4 9 11 13.6 17 21 26 33 41	
flow type	[–]	turbulent	laminar turbulent rough regime	
Re	[–]	10000	1000 4000 100000	$Re_{c,lam}$ $Re_{c,min}$ $Re_{c,max}$
L	[m]	20	5 100	L_{min} L_{max}
r_a	[mm]	75	39 240	$r_{a,min}$ $r_{a,max}$
k	[–]	plastic / steel (inner pipe / outer pipe)	steel / plastic steel / steel plastic / plastic	k_{switch} k_{steel} k_{plast}

Table 3 Used variables

variable	value	unit	source
Re_{lam}	1000	[-]	[15]
Pr	26	[-]	[22]
λ_{steel}	60	[W/(m K)]	[23]
$\lambda_{plastic}$	0.42	[W/(m K)]	[23]
λ_{brine}	0.513	[W/(m K)]	[22]
k_{steel}	2	[mm]	[19]
$k_{plastic}$	0.0015	[mm]	[19]
ρ	1036	[kg/m^3]	[22]
ν	3.35×10^{-6}	[m^2/s]	[22]
c_p	3880	[J/(kg K)]	[22]
T_{earth}	10	[°C]	

Additional Files

Thermal results table

Hydraulic result tables

Table 4 Thermal Results as total borehole resistance R_b^* $[\mathrm{mm\,K/W}]$ for several scenarios

c [-]	λ [W/mK]				L [m]		SDR [-]		r_o [m]		Re_c [-]	
	stand.	switch	plastic	steel	100	5	6	41	min	max	$4 \cdot 10^3$	10^5
	laminar											
0.010	56.94	104.03	104.03	56.94	92.67	35.06	56.94	56.94	70.38	37.79		
0.108	49.55	96.66	96.64	49.56	71.56	31.88	49.54	49.56	58.82	34.19		
0.206	44.81	91.94	91.90	44.85	63.43	29.32	44.78	44.83	52.58	31.36		
0.304	40.30	87.47	87.40	40.38	56.34	26.77	40.26	40.35	46.88	28.56		
0.402	35.74	82.95	82.84	35.85	49.35	24.12	35.70	35.80	41.20	25.66		
0.500	31.01	78.25	78.11	31.16	42.23	21.34	30.97	31.09	35.38	22.62		
0.598	26.04	73.30	73.14	26.20	34.93	18.35	25.99	26.11	29.36	19.36		
0.696	20.72	68.00	67.82	20.90	27.41	15.09	20.68	20.79	23.04	15.81		
0.794	14.96	62.24	62.05	15.14	19.66	11.42	14.91	15.01	16.37	11.82		
0.892	8.56	55.84	55.66	8.74	11.69	7.05	8.52	8.62	9.25	7.12		
0.990	1.25	48.53	48.35	1.43	3.47	1.13	1.22	1.32	1.57	0.92		
	turbulent											
0.010	2.64	49.74	49.74	2.64	2.73	2.51	2.64	2.64	2.72	2.32	6.94	0.65
0.108	3.61	50.72	50.71	3.62	3.79	3.45	3.61	3.62	3.71	3.26	8.27	0.78
0.206	3.88	50.99	50.98	3.90	4.05	3.71	3.88	3.89	3.98	3.53	8.39	0.82
0.304	3.95	51.07	51.05	3.97	4.10	3.79	3.95	3.96	4.04	3.60	8.18	0.83
0.402	3.87	50.99	50.97	3.89	4.01	3.73	3.87	3.88	3.96	3.54	7.74	0.82
0.500	3.65	50.77	50.75	3.68	3.77	3.53	3.65	3.66	3.73	3.34	7.08	0.79
0.598	3.30	50.42	50.40	3.33	3.40	3.21	3.30	3.30	3.37	3.00	6.22	0.74
0.696	2.81	49.93	49.90	2.84	2.89	2.74	2.81	2.81	2.88	2.53	5.15	0.67
0.794	2.17	49.30	49.27	2.20	2.24	2.13	2.17	2.18	2.23	1.92	3.87	0.59
0.892	1.39	48.52	48.48	1.42	1.44	1.37	1.38	1.39	1.44	1.15	2.35	0.48
0.990	0.44	47.59	47.54	0.49	0.48	0.44	0.44	0.44	0.49	0.21	0.55	0.35

Table 5 Hydraulic results as optimal dimensionless inner pipe ratio over different Standard Dimension Ratios (SDR) and different cases (r.r. = rough regime)

Mat.	r_a	SDR									
		6	7.4	9	11	13.6	17	21	26	33	41
		laminar									
-	-	0.6321	0.6121	0.5977	0.5862	0.5767	0.5690	0.5632	0.5586	0.5546	0.5517
		turbulent									
plastic	r_{min}	0.7111	0.6901	0.6749	0.6627	0.6524	0.6440	0.6378	0.6327	0.6283	0.6252
	r_m	0.7110	0.6901	0.6749	0.6626	0.6524	0.6440	0.6377	0.6327	0.6283	0.6251
	r_{max}	0.7109	0.6900	0.6748	0.6626	0.6523	0.6439	0.6377	0.6327	0.6283	0.6251
steel	r_{min}	0.7134	0.6923	0.6769	0.6645	0.6542	0.6456	0.6393	0.6342	0.6297	0.6265
	r_m	0.7149	0.6938	0.6784	0.6659	0.6556	0.6470	0.6407	0.6355	0.6311	0.6278
	r_{max}	0.7161	0.6948	0.6794	0.6669	0.6565	0.6479	0.6415	0.6364	0.6319	0.6287
stand.	r_{min}	0.6651	0.6441	0.6289	0.6167	0.6066	0.5983	0.5921	0.5872	0.5828	0.5797
	r_m	0.6779	0.6570	0.6419	0.6297	0.6196	0.6113	0.6052	0.6002	0.5959	0.5928
	r_{max}	0.6946	0.6739	0.6588	0.6467	0.6366	0.6283	0.6221	0.6172	0.6128	0.6097
switch	r_{min}	0.7303	0.7097	0.6946	0.6824	0.6723	0.6639	0.6576	0.6526	0.6481	0.6450
	r_m	0.7291	0.7083	0.6931	0.6809	0.6706	0.6622	0.6559	0.6508	0.6464	0.6432
	r_{max}	0.7256	0.7045	0.6892	0.6767	0.6664	0.6578	0.6514	0.6463	0.6418	0.6386
		turbulent rough regime									
plastic	r_{min}	0.7223	0.7012	0.6858	0.6733	0.6629	0.6543	0.6480	0.6428	0.6383	0.6351
	r_m	0.7226	0.7014	0.6860	0.6736	0.6632	0.6546	0.6482	0.6431	0.6386	0.6354
	r_{max}	0.7230	0.7019	0.6865	0.6740	0.6636	0.6550	0.6487	0.6435	0.6390	0.6358
steel	r_{min}	0.7137	0.6926	0.6773	0.6649	0.6545	0.6460	0.6397	0.6346	0.6301	0.6269
	r_m	0.7156	0.6944	0.6791	0.6666	0.6563	0.6477	0.6414	0.6363	0.6318	0.6286
	r_{max}	0.7178	0.6967	0.6813	0.6688	0.6585	0.6499	0.6436	0.6384	0.6339	0.6307
stand.	r_{min}	0.6330	0.6100	0.5936	0.5805	0.5696	0.5607	0.5542	0.5489	0.5443	0.5410
	r_m	0.6413	0.6184	0.6020	0.5888	0.5780	0.5691	0.5625	0.5572	0.5526	0.5493
	r_{max}	0.6529	0.6301	0.6137	0.6005	0.5897	0.5808	0.5742	0.5689	0.5642	0.5609
switch	r_{min}	0.7312	0.7106	0.6956	0.6835	0.6734	0.6650	0.6588	0.6538	0.6494	0.6462
	r_m	0.7307	0.7100	0.6950	0.6828	0.6727	0.6643	0.6581	0.6530	0.6486	0.6455
	r_{max}	0.7300	0.7093	0.6942	0.6820	0.6718	0.6634	0.6571	0.6521	0.6477	0.6445

Table 6 Approximation of hydraulic results following the scheme $c_{opt}(SDR) = \frac{m}{SDR} + b$

case material	r_a	parameters regression slope m	intercept b	RMSE
		laminar		
-	-	0.5604	0.5367	0.0011
		turbulent		
plastic	r_{min}	0.5996	0.6093	0.0010
	r_m	0.5994	0.6093	0.0010
	r_{max}	0.5992	0.6093	0.0010
steel	r_{min}	0.6068	0.6105	0.0009
	r_m	0.6081	0.6118	0.0009
	r_{max}	0.6099	0.6126	0.0010
stand.	r_{min}	0.5954	0.5639	0.0011
	r_m	0.5935	0.5770	0.0010
	r_{max}	0.5927	0.5940	0.0010
switch	r_{min}	0.5959	0.6293	0.0009
	r_m	0.5997	0.6274	0.0009
	r_{max}	0.6074	0.6226	0.0009
		turbulent rough regime		
plastic	r_{min}	0.6092	0.6191	0.0009
	r_m	0.6092	0.6193	0.0009
	r_{max}	0.6092	0.6198	0.0009
steel	r_{min}	0.6064	0.6109	0.0009
	r_m	0.6073	0.6126	0.0009
	r_{max}	0.6082	0.6147	0.0009
stand.	r_{min}	0.6407	0.5238	0.0013
	r_m	0.6414	0.5321	0.0013
	r_{max}	0.6412	0.5438	0.0012
switch	r_{min}	0.5933	0.6306	0.0009
	r_m	0.5950	0.6298	0.0009
	r_{max}	0.5973	0.6288	0.0009

Figures

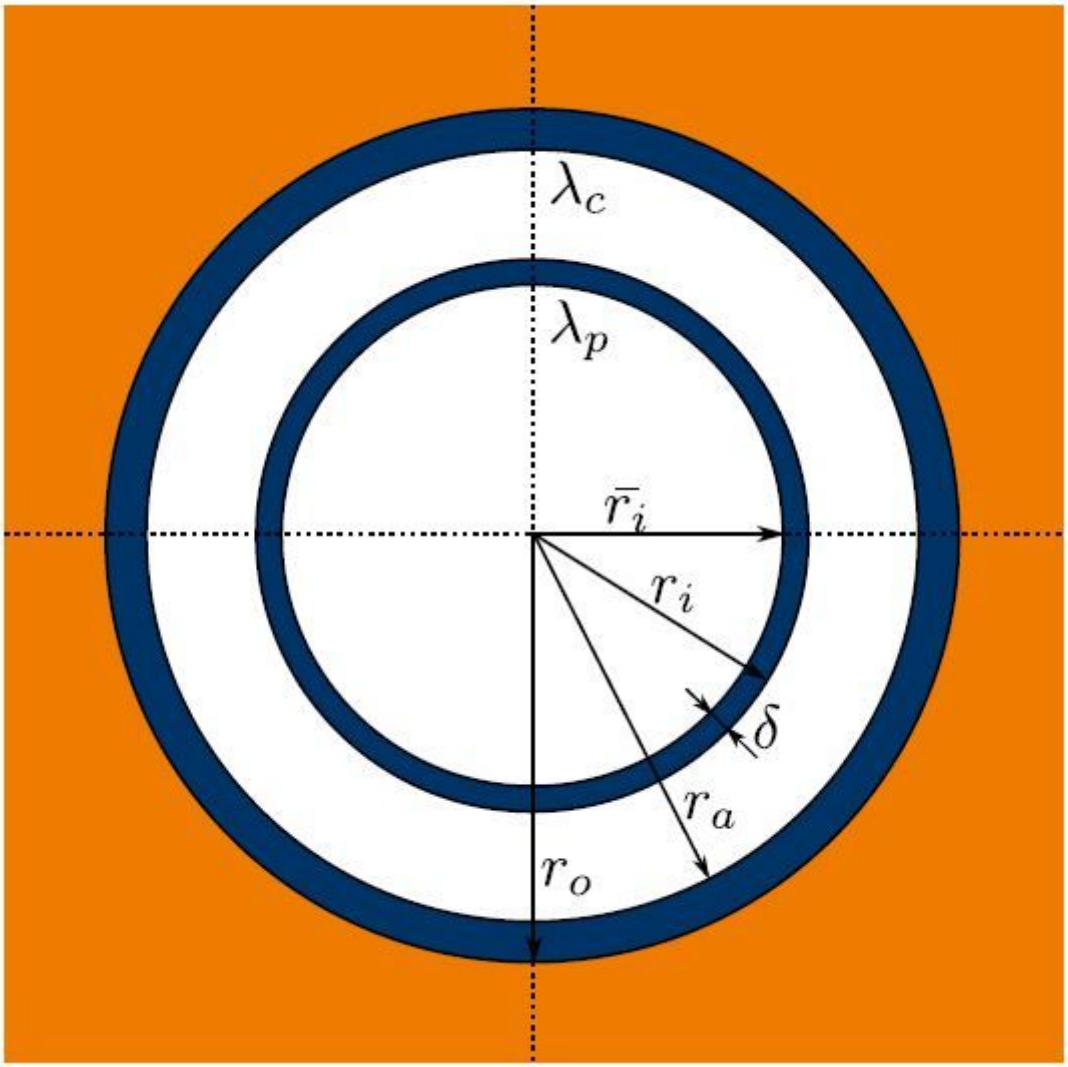

Figure 1

Sketch of a coaxial geothermal heat exchanger with an outer radius of inner pipe (ri), an inner pipe thickness (), inner radius of inner pipe (ri) and an inner radius of outer pipe (ra) as well as an inner pipe thermal conductivity (λp) and an outer pipe thermal conductivity (λc).

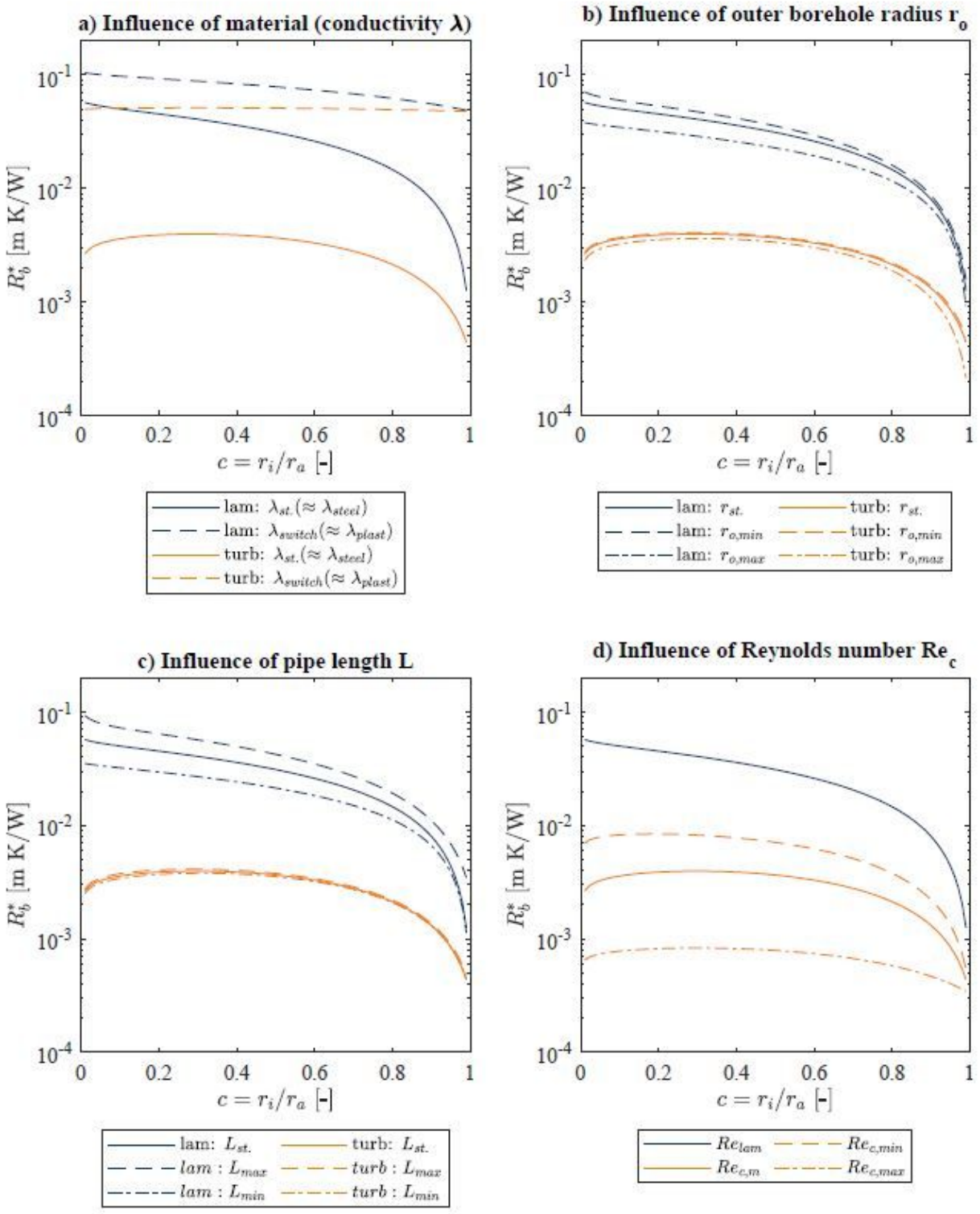

Figure 2

Thermal results Influence of several parameters on thermal performance according to [10] for laminar and turbulent flows a) Total borehole resistance for different materials over dimensionless inner pipe radius c. b) Total borehole resistance for different outer pipe radii ro over dimensionless inner pipe radius c. c) Total borehole resistance for different probe lengths L over dimensionless inner pipe radius c. d)

Total borehole resistance for different Reynolds numbers in the circular ring Rec over dimensionless inner pipe radius c.

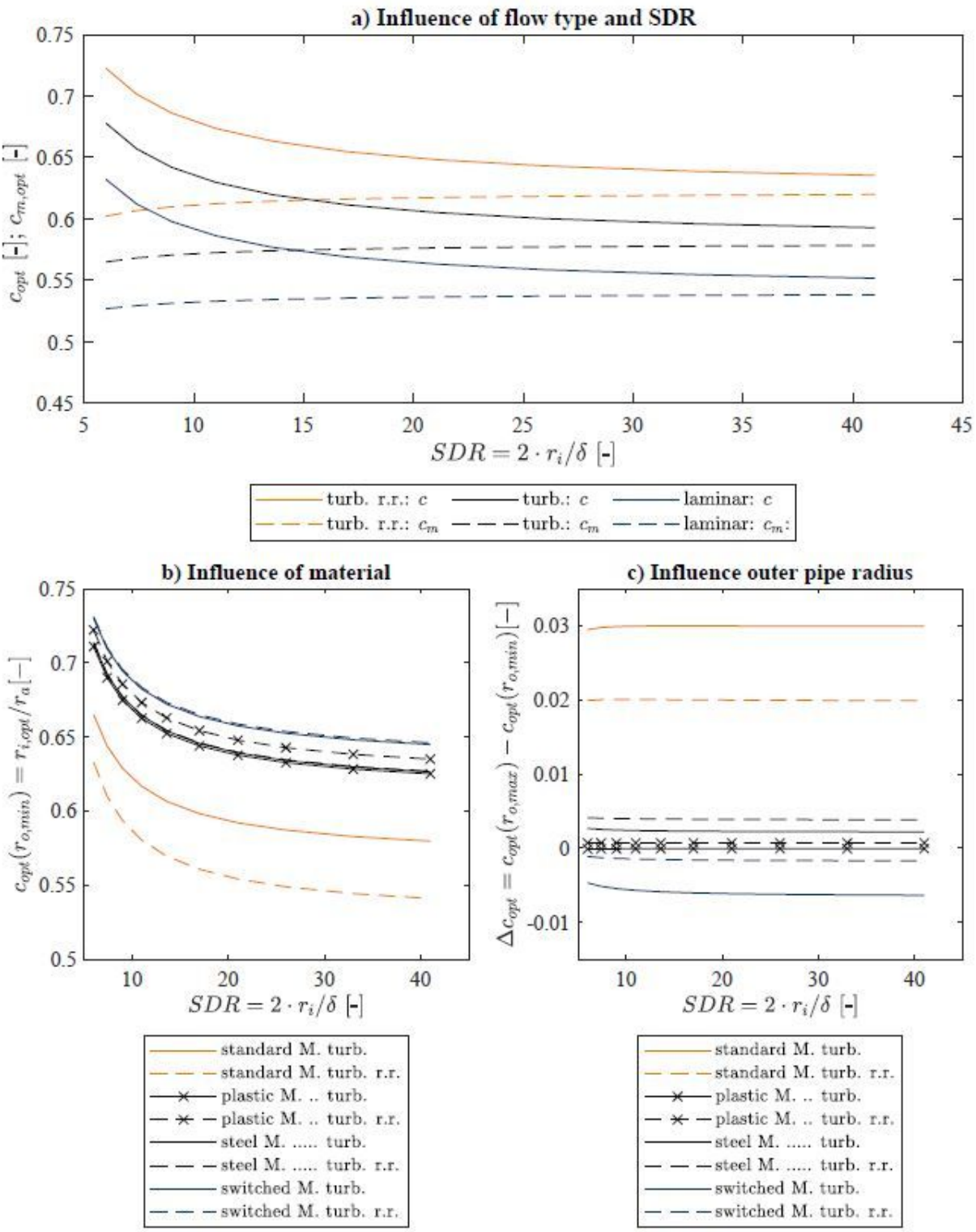

Figure 3

Results of hydraulic optimization Influence of several parameters on optimal hydraulic results for laminar and turbulent flows a) Optimal inner pipe radius copt as well as optimal inner pipe middle radius cm;opt for different flow types over standard dimension ratio SDR. Reference case. b) Optimal inner pipe radius

copt calculated with the smallest outer pipe radius ro;min for all material combinations over SDR c) Deviation copt of optimal inner pipe radius from the results in b) when calculating with the largest outer pipe radius ro;max for all material combinations over SDR.

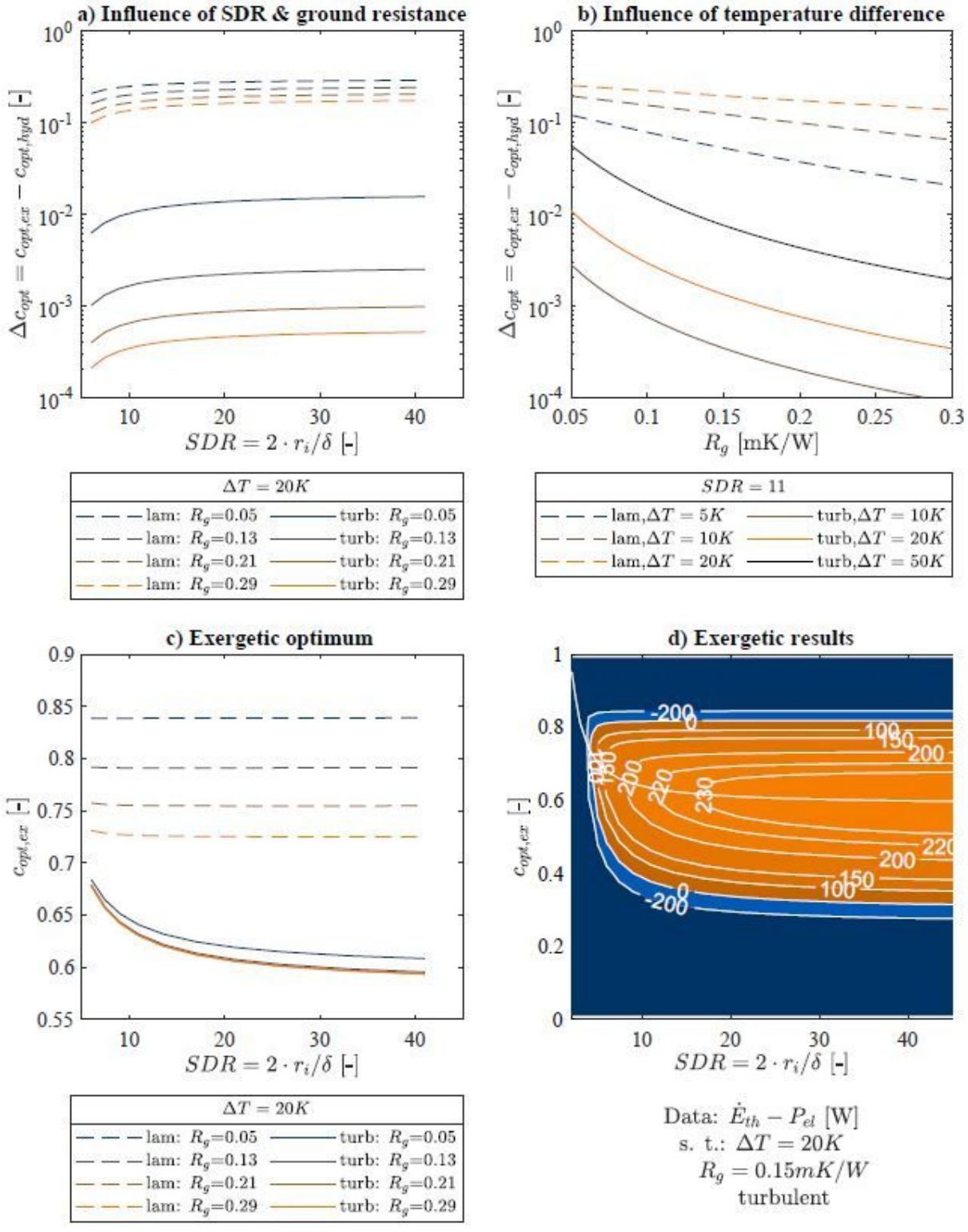

Figure 4

Exergetic results for laminar and turbulent flows a) Change of optimal inner to outer pipe ratio (copt) compared to hydraulic results over Standard Dimension Ratio (SDR) and ground resistance (Rg) b)

Change of optimal inner to outer pipe ratio (copt) over ground resistance (Rg) and Temperature difference(T). c) optimal inner to outer pipe ratio (copt) over Standard Dimension Ratio (SDR) and ground resistance (Rg) d) Exemplary distribution of objective function over the range of c and determined optimum copt